SNITCH: Seeking a simple, comparative SFH inference tool

R. J. Smethurst,[1] C. J. Lintott,[2] et al.

[1] *School of Physics and Astronomy, The University of Nottingham, University Park, Nottingham, NG7 2RD, UK*
[2] *Oxford Astrophysics, Department of Physics, University of Oxford, Denys Wilkinson Building, Keble Road, Oxford, OX1 3RH, UK*

10 January 2018

ABSTRACT

We present SNITCH, an open source code written in *Python*, developed to infer a simple toy model of star formation history of a galaxy spectrum from the emission and absorption features. SNITCH utilises FSPS, the MaNGA DAP and *emcee* in order to provide the inferred $[Z, t_q, \tau]$ parameters with which to describe the exponentially declining quenching history of the input spectral features. This code was written for use on the MaNGA spectral data cubes but can be used for any scenario where a spectrum has been obtained, or spectral feature measurements have been provided. This code is not intended for an accurate inference of a single spectrum SFH but as a comparison of SFHs across many different spectra, either in an IFU scenario or across a galaxy population.

Key words: software – description

1 INTRODUCTION

Whilst there are many codes which provide a full spectral fit to a galaxy spectrum in order to determine its SFH, there are few providing a simpler, quicker inference of a toy model of star formation history (SFH).

Here we present an open source *Python* software which uses Bayesian statistics and MCMC methods to infer a simple toy model of SFH from the absorption and emission features of a galaxy (or IFU) spectrum.

Herein we describe our SFH inference code, SNITCH (bayeSian iNference given emIssion and absorpTion features of quenChing Histories), in Section 2, the expected output of the code in Section 3, along with the rigorous testing procedures applied to SNITCH in Section 4. Where necessary we adopt the Planck 2015 (Planck Collaboration et al. 2016) cosmological parameters with $(\Omega_m, \Omega_\lambda, h) = (0.31, 0.69e, 0.68)$.

2 DESCRIPTION OF CODE

Simply put, SNITCH takes absorption and emission spectral features and their associated errors as inputs, assumes a simple SFH model and convolves it with a SPS to generate a synthetic spectra. These synthetic spectra are then fitted to give resulting prediced absorption and emission spectral features which the code uses to infer the best fit model using Bayesian statistics and MCMC methods given the spectral inputs.

We describe this process below, first defining our toy model of SFH, describing how we convolve this with SPS models to produce synthetic spectra (Section 2.2), how these spectra are then fitted to provide predicted model spectral features (Section 2.3) and then how these are used to infer the best fit SFH given the input parameters (Section 2.5).

2.1 Star Formation History Model

The SFH used in this code was first described in Smethurst et al. (2015). We have reproduced its descroption here. The quenched star formation history of a galaxy can be simply modelled as an exponentially declining star formation rate (SFR) across cosmic time as:

$$SFR = \begin{cases} I_{sfr}(t_q) & \text{if } t \leqslant t_q \\ I_{sfr}(t_q) \times exp\left(\frac{-(t-t_q)}{\tau}\right) & \text{if } t > t_q \end{cases} \quad (1)$$

where t_q is the onset time of quenching, τ is the timescale over which the quenching occurs and I_{sfr} is an initial constant star formation rate dependent on t_q. A smaller τ value corresponds to a rapid quench, whereas a larger τ value corresponds to a slower quench. This model is clearly not a fully hydrodynamical simulation, it is a deliberately simple model built in order to test our understanding of the evolution of galaxy populations. This SFH model has previously been shown to appropriately characterise quenching galaxies (Weiner et al. 2006; Martin et al. 2007; Noeske & et al. 2007; Schawinski et al. 2014). For galaxies which are still star forming, this model results in a constant SFR.

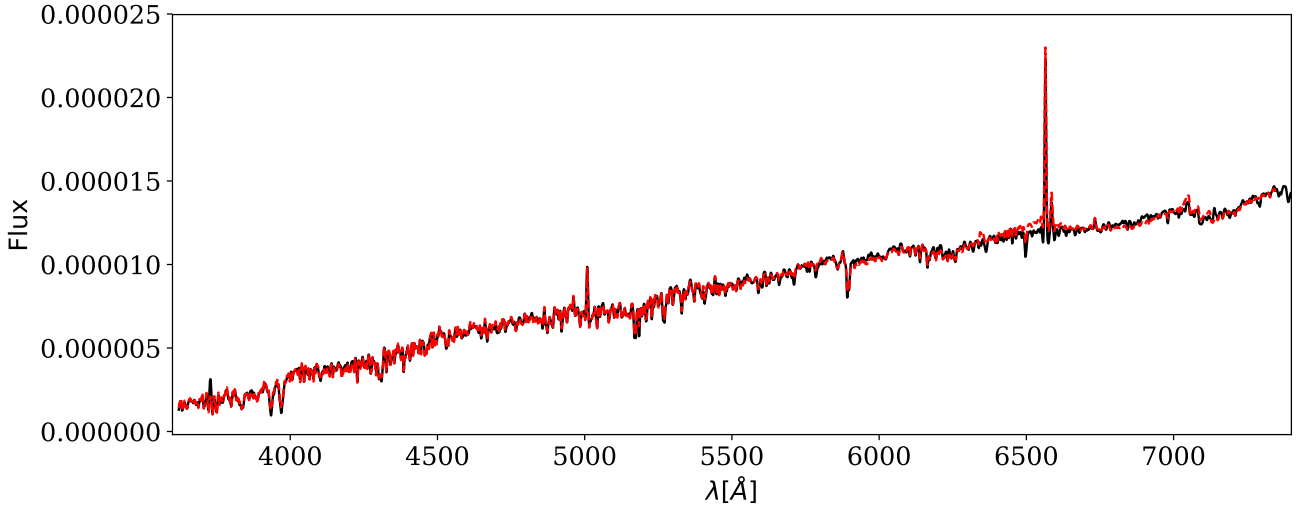Here, I assume that all galaxies formed at a time $t =$

Figure 1. Example synthetic spectra constructed using FSPS, shown by the black solid line, along with the fit returned by the MaNGA DAP (i.e. ppxf, emission lines and absorption features) shown by the red dashed line.

0 Gyr with an initial burst of star formation, $I_{sfr}(t_q)$. This initial constant star formation rate must be defined in order to ensure the 'model' galaxy has a reasonable stellar mass by $z \sim 0$. This value will be dependent on the epoch at which quenching is modelled to occur, hence the dependence of this initial star formation rate on quenching time in Equation 1. To tackle this problem, I looked to the literature; Peng & et al. (2010, Equation 1) define a relation between the average specific SFR (sSFR = SFR/M_*) and redshift by fitting to measurements of the mean sSFR of blue star forming galaxies from SDSS, zCOSMOS and literature values from Elbaz et al. (2007) and Daddi et al. (2007) measured at increasing redshifts with data from the GOODS survey:

$$sSFR(m,t) = 2.5 \left(\frac{m}{10^{10} M_\odot} \right)^{-0.1} \left(\frac{t}{3.5 \text{ Gyr}} \right)^{-2.2} \text{Gyr}^{-1}.$$
(2)

Beyond $z \sim 2$ the characteristic SFR flattens and is roughly constant back to $z \sim 6$. This flattening can be seen across similar observational data (Peng & et al. 2010; González et al. 2010; Béthermin et al. 2012); the cause is poorly understood but may reflect a physical limit to the sSFR of a galaxy.

Motivated by these observations, the relation defined in Peng & et al. (2010) is taken up to a cosmic time of $t = 3$ Gyr ($z \sim 2.3$) and prior to this the value of the sSFR at $t = 3$ Gyr is used. At the point of quenching, t_q, the SFH models are therefore defined to have an $I_{sfr}(t_q)$ which lies on this relationship for the sSFR, for a galaxy with mass, $m = 10^{10.27} M_\odot$. This choice of $I_{sfr}(t_q)$ is an important one, however does not impact on the predicted spectral features output by the model as it is merely a normalisation factor on the SFH. $[t_q, \tau]$, which set the shape of the SFH, and Z which can affect the strength of a spectral feature are the crucial parameters.

2.2 Synthetic spectra generation

We then employ stellar population synthesis models (SPS) in order to construct synthetic spectra with the SFHs defined in Section 2.1. These synthetic spectra will be measured the same as an observed spectra (see Section 2.3) in order to make a direct comparison using Bayesian statistics (see Section 2.5) to determine the 'best fit' SFH model for a given spectral features input.

In order to derive a realistic synthetic spectra with our defined SFHs we utilised the Flexible Stellar Population Synthesis (FSPS) Model[1] code of Conroy et al. (2009); Conroy & Gunn (2010), which is written in `FORTRAN`, in conjunction with an existing *Python* wrapper[2] by Foreman-Mackey et al. (2014). SPS methods rely on stellar evolution calculations during all stages of stellar life, stellar spectral libraries, dust models and initial mass functions (IMFs) to translate the evolution of a hypothetical number of stars of varying ages and metallicities into a predicted integrated spectrum. FSPS also integrates `CLOUDY` (Ferland et al. 2013) into its output so that stellar emission lines can also be synthesised along with a stellar continuum.

The FSPS Python wrapper makes it possible to generate spectra (or magnitudes) for any arbitrary stellar population in just two lines of *Python* code. For example:

```
sp = fsps.StellarPopulation(
        zmet=18, sfh=3,
        dust_type=2, imf_type=1,
        add_neb_emission=True,
        add_dust_emission=True)
sp.set_tabular_sfh(age = ages, sfr=sfrs)
```

In SNITCH we set up the FSPS models to produce spectra using the Padova isochrones (Girardi et al. 2002) and

---

[1] https://github.com/cconroy20/fsps
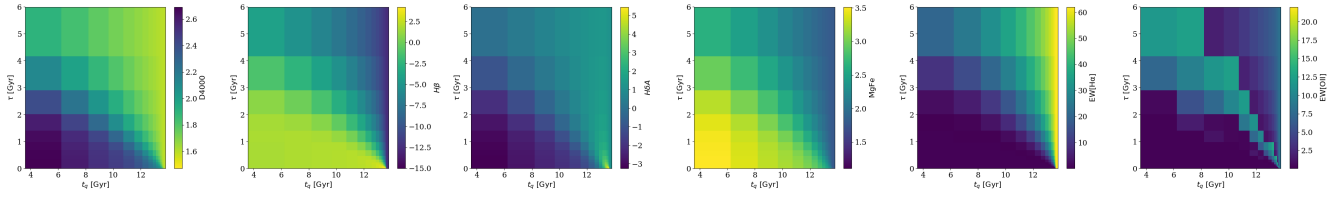[2] http://dfm.io/python-fsps/current/

Figure 2. The variation of model spectral features across the logarithmically binned two dimensional $[t_q, \tau]$ parameter space measured at $t_{obs} = 13.6$Gyr and solar metallicity, $Z = Z_\odot$. The features shown from left to right are the D4000, Hβ, Hδ_A and MgFe' spectral absorption indices and the equivalent width of both $H\alpha$ and $[OII]$ emission lines. This figure shows how each feature is sensitive to the changing SFH and how they can be used to break the degeneracies that plague photometric studies of SFH.

MILES spectral library (Vazdekis et al. 2016) with neb-ular emission, emission from dust Draine & Li (2007), a Chabrier (2003) IMF and a Calzetti et al. (2000) dust ex-tinction curve. We also smooth the generated synthetic spec-tra to have the minimum velocity dispersion measurable by MaNGA, 77 km s^{-1} (Bundy & et al. 2015). Spectra are gen-erated for the 22 metalicities provided in the MILES models, ranging from 0.011 $Z_\odot$ to 1.579 $Z_\odot$ across a logarithmic age range spanning the Universe's history. FSPS does not allow for chemical enrichment of stellar birth material with time, i.e. the metallicity is kept constant for a given SFH at all epochs.[3] These spectra are generated across a 4-dimensional array in $[t_{obs}, Z, t_q, \tau]$in order to facilitate faster run time during inference (see Section 2.5).

An example synthetic spectra generated with FSPS for solar metallicity, with a $t_q = 10$ Gyr, $\tau = 1.0$ Gyr observed at a redshift, $z = 0.1$ (i.e. $t_{obs} = 12.1$ Gyr) is shown by the solid black line in Figure 1.

2.3 Measuring the synthetic spectral features

This code was originally developed for a specific science case using MaNGA IFU survey data (an integral-field spectro-scopic survey of 10,000 galaxies undertaken by the fourth phase of the Sloan Digital Sky Survey, SDSS-IV; Bundy & et al. 2015). We therefore wished to measure our synthetic spectra generated using FSPS (see Section 2.2) in the same way as the MaNGA data. It is for that reason that we use the functions defined in the MaNGA Data Analysis Pipeline (DAP; Westfall prep) version 2.0.2 in order to measure the features in our synthetic spectra. If the user has a predefined method for measuring emission and absorption features in their spectra, the `measure_spec` function in SNITCH can sim-ply be adapted.

The MaNGA DAP is described in full detail in West-fall (prep), however here we lay out the functions used in SNITCH to fit our synthetic spectra. Firstly we used pPXF (Cappellari & Emsellem 2004) to extract a fit of the stellar continuum of our synthetic spectra. Here we use the version of pPXF coded into the MaNGA DAP using the `PPXFFit` object and the MILES template spectral libraries. Secondly,

we used the obtained stellar continuum to fit the emission line features in the spectra using the `Elric` object and the `"ELPFULL"` emission line database of 26 lines provided in the MaNGA DAP. This procedure provides emission line fluxes, equivalent widths, and kinematics from single component Gaussian fits. All strong lines are fit, as well as the Balmer series up to Hϵ and other weaker lines. Finally, we then fit the absorption indices in our synthetic spectra using the `SpectralIndices` object and the `"EXTINDX"` index database of 42 indices provided in the MaNGA DAP. Spectral-index measurements including the $4000\mathring{A}$ break, TiO bandhead features and the full Lick system. All indices are measured at the MaNGA resolution (specified for each index) and correc-tions are provided to a nominal, $\sigma_v = 0$ measurement. The measurements of the Lick indices are provided by convolving the MaNGA data to the Lick resolution.

2.4 Choosing which spectral features to use

Whilst there are many star formation sensitive spectral fea-tures used previously in the literature () here we adopted a from first principles approach. We observed how each of the 26 emission and 42 absorption features measured by the MaNGA DAP (see Section 2.3), changed across the model parameter space $[Z, t_q, \tau]$ with time of observation to de-termine which spectral features were most sensitive to star formation rate, metallicity, time of observation etc.

We looked at plots similar to those shown in Figure 2 for all 26 emission features and 42 absorption features and selected the following features with which to infer the SFH:

(i) EW[Hα] as it is the most sensitive to current star formation rate

(ii) EW[OII] as it is the most sensitive to stars that are ~ 1 Gyr old

(iii) D4000 as it is most sensitive to the age of the stellar popu-lation

(iv) Hβ as it is most sensitive to the metallicity of the stellar population irrespective of the population age

(v) Hδ_A as it is the most sensitive to A-stars and therefore star formation that has been cut off abruptly in the recent past

(vi) MgFe' as it is most sensitive to the metallicity of the stellar population irrespective of the current star formation rate

Each of these features is measured in the synthetic to spectra in order for the input values to be compared to model values to find the best fit SFH. Not all six features need to be measured in a spectrum for SNITCH to run, although not providing one as input does restrict the accuracy to which

[3] Whilst we could attempt to provide a feature to implement chemical enrichment into these models this would firstly be full of uncertainty (the propagation of which would be unquantifiable) and secondly move us out of the regime of a toy SFH model and into hydrodynamic simulation territory.

a SFH can be inferred (see Section **??**). An estimate of the error on these measured values is also needed for SNITCH to run.

2.5 Bayesian inference of SFH parameters

For the SFH problem at hand, using a Bayesian approach requires consideration of all possible combinations of the model parameters $\theta \equiv [Z, t_q, \tau]$ (the hypothesis in this instance). Assuming that all galaxies formed at $t = 0$ Gyr, we can assume that the 'age' of a spectrum is equivalent to an observed time, t_k^{obs}. I then used this 'age' to calculate the *predicted*, p, spectral features at this cosmic time for a given combination of θ: $\vec{d}_{s,p}(\theta_k, t_k^{obs})$ for each of the six spectral features: EW[Hα], EW[OII], D4000, Hβ, Hδ_A and $MgFe'$. The predicted spectral features can now directly be compared with input observed spectral features, so that for a single spectrum k with features $\vec{d}_k = \{s_k\}$, with length S, the likelihood of a given model $P(d_k|\theta_k, t_k^{obs})$ to be:

$$P(\vec{d}_k|\theta_k, t_k^{obs}) =$$
$$\prod_{s=1}^{S} \frac{1}{\sqrt{2\pi\sigma_{s,k}^2}} \exp\left[-\frac{(d_{s,k} - d_{s,p}(\theta_k, t_k^{obs}))^2}{\sigma_{s,k}^2} \right] \quad (3)$$

Here I have assumed that $P(d_{s,k}|\theta_k, t_k^{obs})$ are all independent of each other and that the errors on the observed features, $\sigma_{s,k}$, are also independent (a simplifying assumption but difficult to otherwise constrain). To obtain the probability of a combination of θ values given the data: $P(\theta_k|\vec{d}_k, t^{obs})$, i.e. how likely a single SFH model is given the observed spectral features of a spectrum, I utilise Bayes' theorem as:

$$P(\theta_k|\vec{d}_k, t^{obs}) = \frac{P(\vec{d}_k|\theta_k, t^{obs})P(\theta_k)}{\int P(\vec{d}_k|\theta_k, t^{obs})P(\theta_k)d\theta_k}. \quad (4)$$

I assume a flat prior on the model parameters so that:

$$P(\theta_k) = \begin{cases} 1 & \text{if } 0 < Z[Z_\odot] \leqslant 1.5 \text{ and } 0 < t_q \text{ [Gyr] } \leqslant 13.8 \text{ and } 0 < \tau \text{ [Gyr] } \leqslant 6 \\ 0 & \text{otherwise.} \end{cases} \quad (5)$$

As the denominator of Equation 4 is a normalisation factor, comparison between likelihoods for two different SFH models (i.e., two different combinations of $\theta_k = [Z, t_q, \tau]$) is equivalent to a comparison of the numerators. Markov Chain Monte Carlo (MCMC; Mackay 2003; Foreman-Mackey et al. 2013; Goodman & Weare 2010) analysis provides a robust comparison of the likelihoods between θ values.

MCMC allows for a more efficient exploration of the parameter space than a simple χ^2 analysis by avoiding those areas with low likelihood. A large number of 'walkers' are started at an initial position (i.e. an initial hypothesis, θ), where the likelihood is calculated; from there they individually 'jump' a randomised distance to a new area of parameter space. If the likelihood in this new position is greater than the original position then the 'walkers' accept this change in position. Any new position then influences the direction of the 'jumps' of other walkers (this is the case in ensemble MCMC as used in this investigation but not for simple MCMC, which is much slower at converging). This is repeated for the defined number of steps after an initial 'burn-in' phase. The length of this burn-in phase is determined
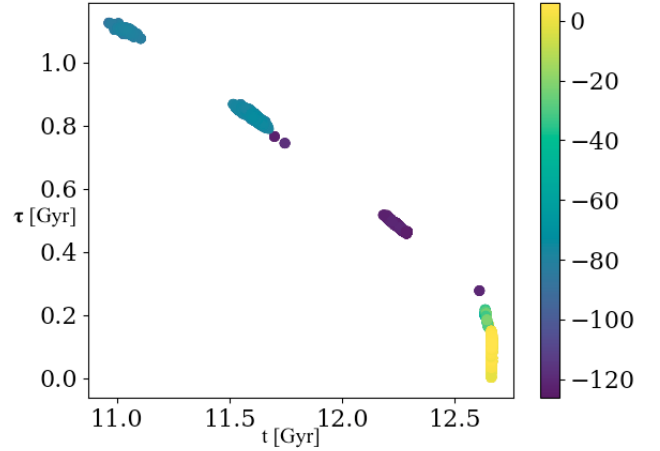

Figure 3. This figure shows the walker positions marginalized over the Z dimension into the two dimensional model $[t_q, \tau]$ space and coloured by their log probability value. The higher the value of their log probability, the more likely the model is. The lower values of log probability for some groups of walkers suggests that these are indeed stuck in local minima. These clusters of walkers in local minima can be 'pruned' (see Section 2.6) away to leave only the global minimum in the final output.

after sufficient experimentation to ensure that the 'walkers' have converged on a region of parameter space. Here we use *emcee*,[4] a *Python* module which implements an affine invariant ensemble sampler to explore the parameter space, written by Foreman-Mackey et al. (2013). *emcee* outputs the positions of these 'walkers' in the parameter space, which are analogous to the regions of high posterior probability.

For each run of SNITCH, the inference run is initialised with 100 walkers with a burn-in phase of 500 steps before a main run of 100 steps. Acceptance fractions for each walker are difficult to estimate due to the fact that walkers often get stuck in local minima during a run (see Section 2.6 for more information).

2.6 Pruning walkers stuck in local minima

After running SNITCH and upon inspection of the walker positions it became apparent that the walkers of *emcee* would often get stuck in local minima. We therefore implemented a pruning method, as described in Hou et al. (2012), in order to remove those walkers in local minima leaving only the global minima from which to derive inferred SFH parameters. The method outlined in Hou et al. (2012) is a simple one dimensional clustering method wherein the average negative log-likelihood for each walker is collected. This results in L numbers:

$$\bar{l}_k = \frac{1}{T} \sum_{t=1}^{T} l(\vec{\theta}_k(t)|D), \quad (6)$$

where T is the total number of steps each walker, k, takes. These L numbers, $\bar{l}_k$ are therefore characteristic of the well
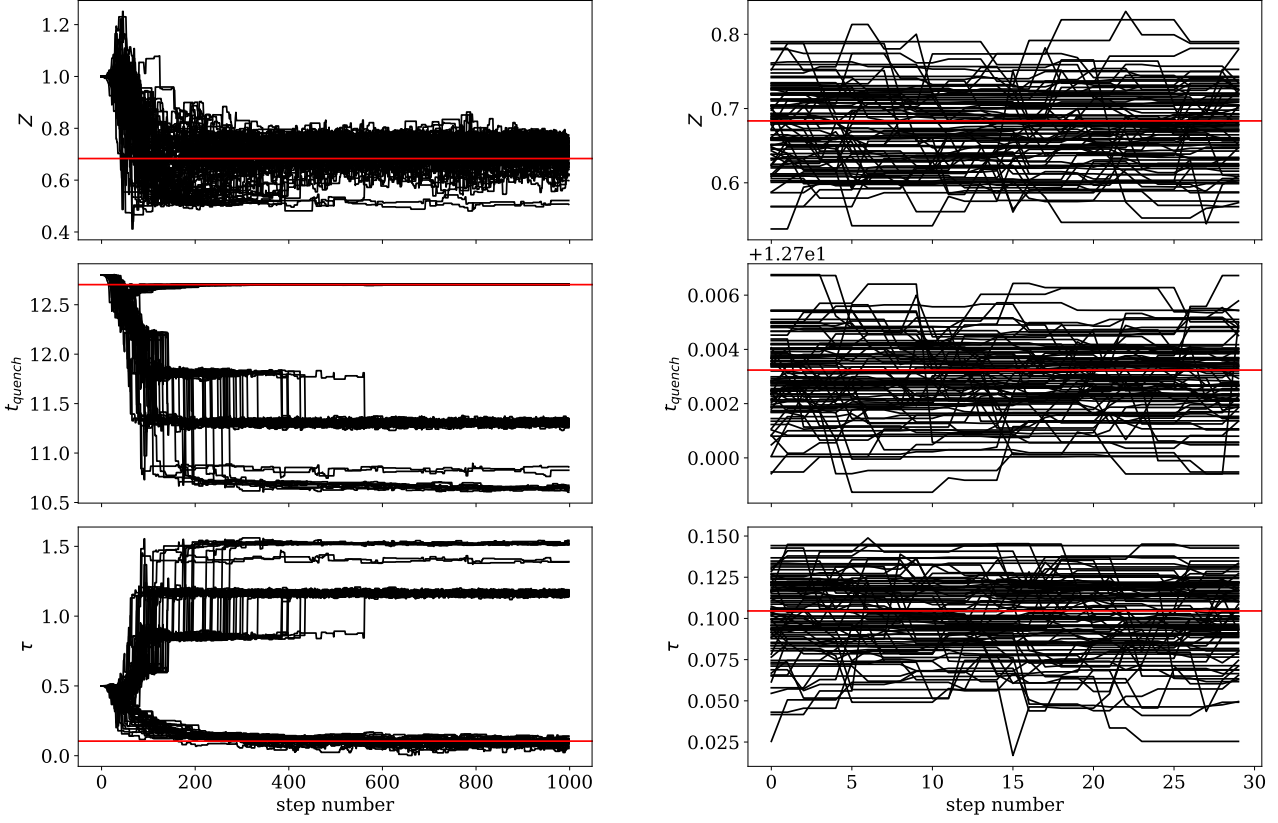
---

[4] dan.iel.fm/emcee/

Figure 4. The positions traced by the *emcee* walkers with step number (i.e. time) in each of the $[Z, t_q, \tau]$ dimensions during the burn in phase before pruning (left) and the post burn-in phase after pruning (right). The red lines show the known true values in each panel. Walkers have got stuck in local minima (see Figure3) but some have managed to find the global minimum which can be seen more clearly in the right hand panels.

which walker k is in, so that walkers in the same well will have similar $\bar{l}_k$ (see Figure 3 in which walkers are coloured by their characteristic $\bar{l}_{(k)}$ value).

The walkers are all then ranked in order of decreasing average log likelihood, $\bar{l}_{(k)}$, or increasing $-\log \bar{l}_{(k)}$. If there are big jumps in the $-\log \bar{l}_{(k)}$, these are easy to spot and are indicative of areas where walkers have got stuck in local minima. The difference in $-\log \bar{l}_{(k)}$ for every adjacent pair of walkers is then calculated. The first pair whose difference is a certain amount times bigger than the average difference previously is then identified like so:

$$-\log \bar{l}_{(j+1)} + \log \bar{l}_{(j)} > Const \frac{\log \bar{l}_{(j)} + log\bar{l}_{(1)}}{j - 1}. \quad (7)$$

All the walkers with with $k > j$ are thrown away and only the ones with $k \leqslant j$ are kept after being identified as part of the global minimum. This can be seen in Figure 4 wherein the walker positions at each step before pruning in the burn-in phase are shown in comparison to those after pruning in the main run stage.

3 OUTPUT OF CODE

The burn-in and main run walker positions and posterior probabilities at each step are written to disc by SNITCH. From this three dimensional MCMC chain charting the $[Z, t_q, \tau]$ positions of the walkers around parameter space, the 'best fit' $[Z, t_q, \tau]$ values along with their uncertainties can be determined from the 16th, 50th and 84th percentile values of the walker positions. An example output from SNITCH for a single synthetic spectrum constructed with the FSPS models (see Section 2.2) is shown in Figure 5. This figure is also written to disc by SNITCH upon completion of a run on a single spectrum.

I used the *Python* programming language to code the routine outlined in Section 2 into a package named SNITCH which has been released with an open source license. The required inputs for SNITCH to run on a single spectrum are at least one, if not all, of EWHα, EW[OII], D4000, Hβ, Hδ_A and MgFe' and their associated errors and the spectrum redshift, z.
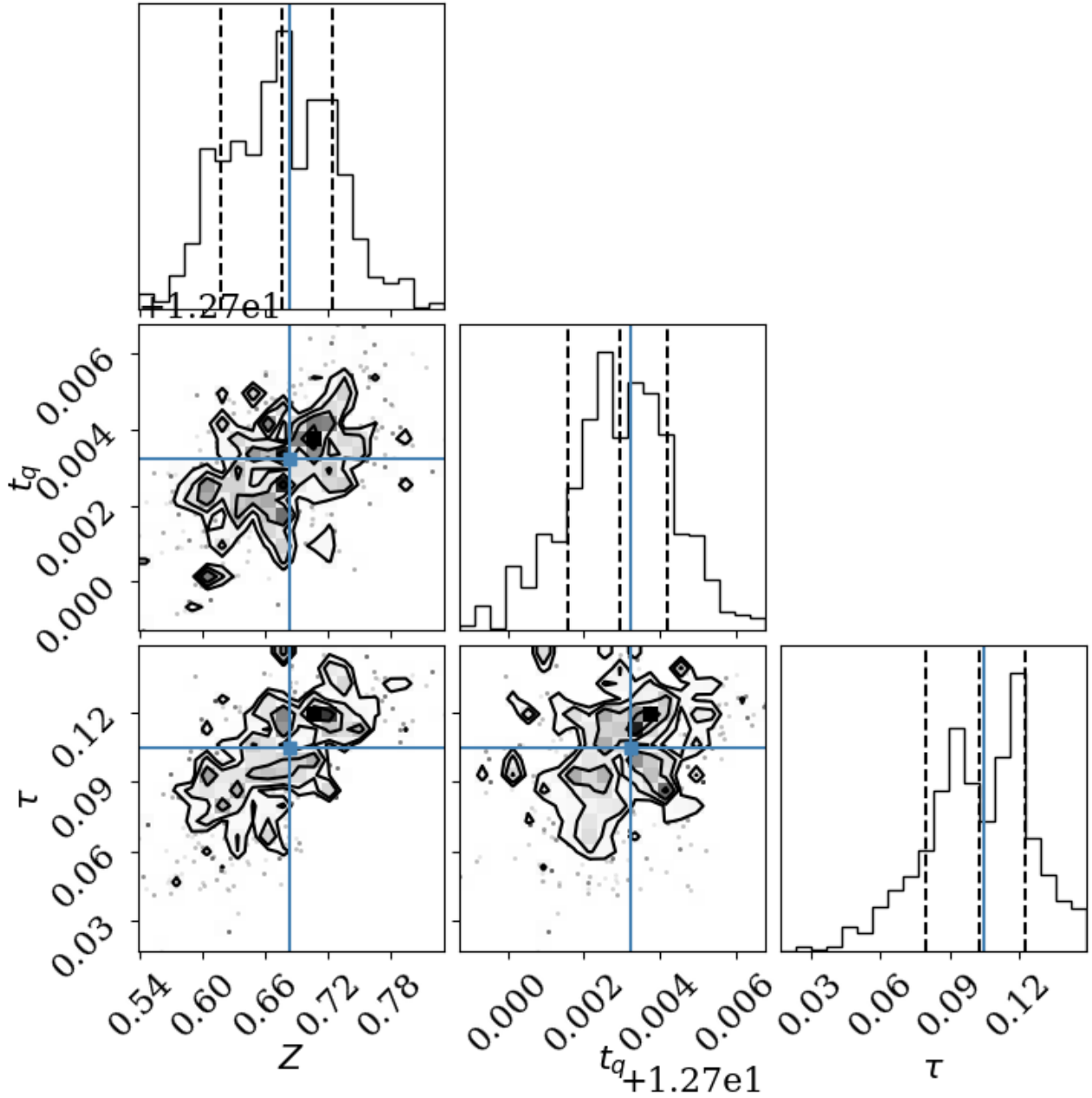
Figure 5. Example output from SNITCH showing the posterior probability function traced by the MCMC walkers across the three dimensional parameter space $[Z, t_q, \tau]$. Dashed lines show the 18th, 50th and 64th percentile of each distribution function which can be interpreted as the 'best fit' with 1σ. The blue lines show the known true values which SNITCH has managed to recover.

4   TESTING

4.1   Testing precision

5   SEC:PRECISIONTEST

In order to test that SNITCH can find the correct quenched SFH model for a given set of spectral features, 25 synthesised galaxy spectra were created with known SFHs (i.e. known values of $\theta = [Z, t_q, \tau]$) from which spectral features were generated using the FSPS models (see Section 2.2. These

were input into SNITCH to test whether the known values of θ were reproduced, within error, for each of the 25 synthesised galaxies. Figure 6 shows the results for each of these synthesised galaxies, with the known values of θ shown by the red lines. In only one case for the τ parameter this red line does not fall within the 16th and 84th percentile values shown by the blue dashed lines (see bottom right panel). However, on inspection, this SFH was a constant SFR that had not yet quenched and so the posterior probability function returned for the τ parameter is very broad as SNITCH
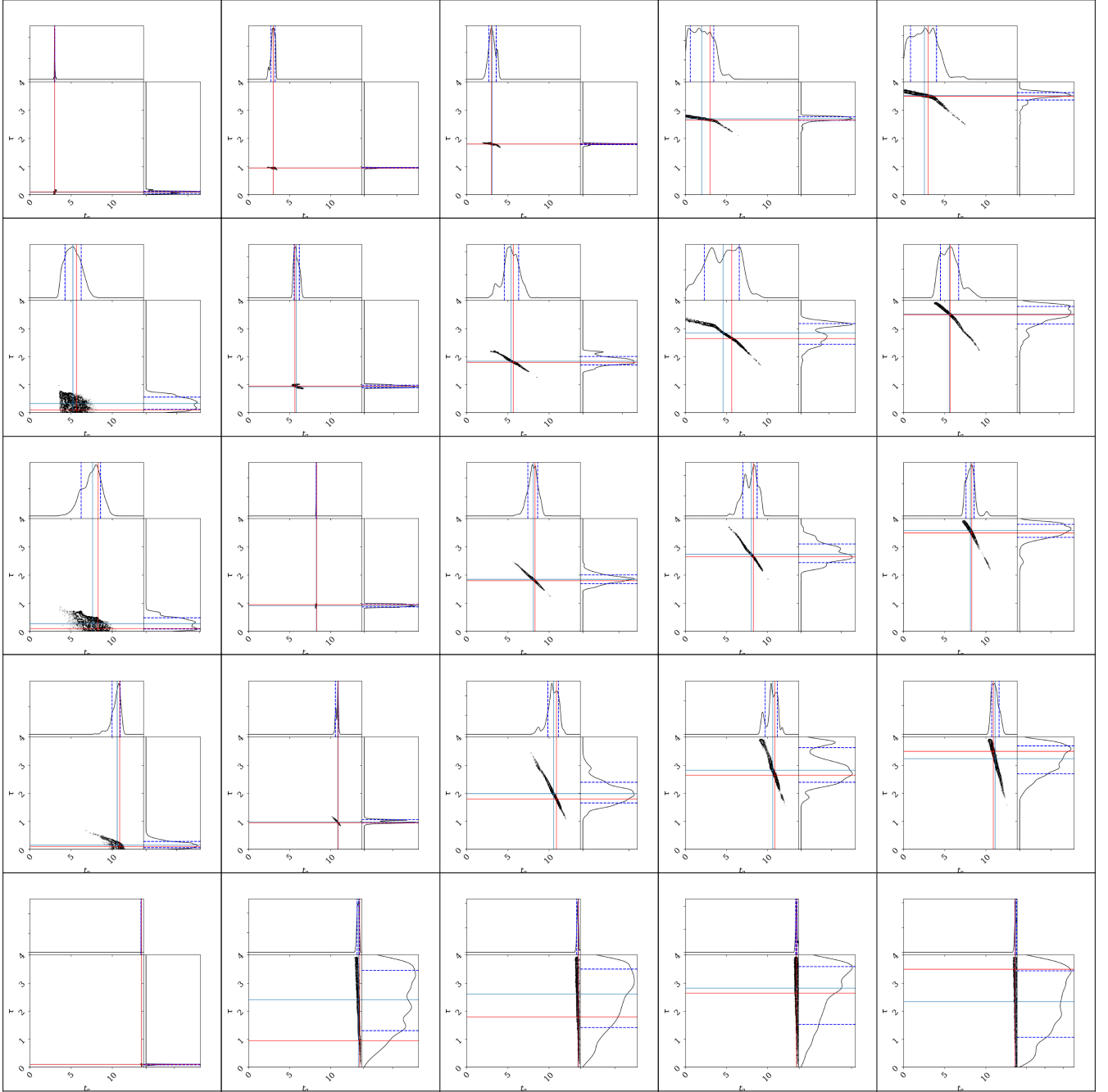
Figure 6. Results from SNITCH for an array of synthesised galaxies with known true $[Z, t_q, \tau]$ values (marked by the solid red lines) assuming an error on the input spectral measurements of the average error on the measured MaNGA spectra measurements. Pruning has been applied? In each case SNITCH has succeeded in locating the true parameter values within the degeneracies of the star formation history model.

does not have any information with which to constrain this parameter. In all cases the intersection of the red lines (i.e. the known or true values input) resides within the parameter space explored by the walkers left over after pruning, which trace the global minimum of the posterior probability. Therefore SNITCH succeeds in precisely locating the true parameter values within the degeneracies of the SFH model for known values.

5.1 Testing precision when less spectral information provided

SNITCH is designed so that not all six of the spectral features have to be provided for the code to return an inferred quenching history. This is a particularly useful feature if the user is unable to obtain or measure a certain spectral feature, if for example, measurements are being obtained from

Table 1. The mean uncertainties ($\pm 1\sigma$) on the best fit for the 25 synthesised galaxy spectra returned when each spectral feature is omitted in turn

Spectral feature omitted	None	Hα	$[OII]$	$D4000$	Hβ	H$\delta_{\rm A}$	MgFe'
Average uncertainty $\pm 1\sigma$							

archival data or a feature lies outside of the wavelength range of their spectrum.

Users should note that quenching histories inferred given less inputs results in a larger uncertainty on the quoted best fit parameters returned by SNITCH. To quantify this we repeated the test described in Section **??** six times, each time omitting one of the spectral features from the list of inputs. The mean uncertainties on the best fit for the 25 synthesised galaxy spectra returned when each spectral feature is omitted are quoted in Table 1.

For further combinations of missing parameters, we suggest the user completes their own tests to determine how the quoted uncertainty will chance with the omission of more than one spectral feature. However, we do not recommend using SNITCH if the number of available spectral features is less than 4. If this is the case, the number of inputs given to the code will be equal to or less than the number of parameters to be inferred and the results will become wildly unreliable.

5.2 Testing accuracy

We have shown in the previous section that SNITCH is precise in returning known values for SFHs, however how can we be sure that it is returning an accurate result?

5.3 Testing performance with different known SFHs

Obviously, not all galaxies will be accurately described by an exponentially quenching SFH. In special use cases (for example studying post starburst galaxies) a different SFH may be defined by the user by replacing the `expsfh` function with their own.

However, we have also tested how SNITCH behaves when known SFHs of different shapes to the exponentially quenching model it assumes are input. We tested a constant, burst, many burst, normal and log-normal models of SFH (see Figure 7) all of which are often used in the literature to model simple SFHs.

We found that SNITCH was always sensitive to the most recent epoch of star formation or quenching. For the constant SFR model, SNITCH returned a very recent t_q and a very large τ, i.e. a galaxy which has had constant SFR up until very recently at which point it started to decline very slowly. For the burst and many-burst models, SNITCH returns a constant SFR up until the peak of the last burst at which point quenching happens very rapidly. Similarly for the log normal and normal SFHs, SNITCH returns a best fit SFH with constant SFR until the peak of the normal and which point it declines at a rate comparable to the drop off of the Gaussian SFH.
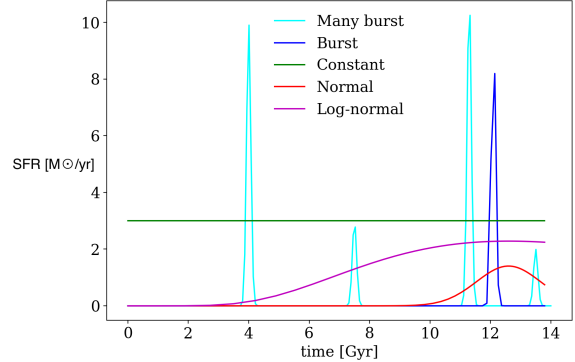
Figure 7. The shapes of the different known SFHs input into SNITCH.

5.4 Testing against previously derived SFHs

6 CONCLUSIONS

REFERENCES

Béthermin M., Daddi E., Magdis G., Sargent M. T., Hezaveh Y., Elbaz D., Le Borgne D., Mullaney J., Pannella M., Buat V., Charmandaris V., Lagache G., Scott D., 2012, ApJ, 757, L23

Bundy K., et al. 2015, ApJ, 798, 7

Calzetti D., Armus L., Bohlin R. C., Kinney A. L., Koornneef J., Storchi-Bergmann T., 2000, ApJ, 533, 682

Cappellari M., Emsellem E., 2004, PASP, 116, 138

Chabrier G., 2003, PASP, 115, 763

Conroy C., Gunn J. E., 2010, ApJ, 712, 833

Conroy C., Gunn J. E., White M., 2009, ApJ, 699, 486

Daddi E., Dickinson M., Morrison G., Chary R., Cimatti A., Elbaz D., Frayer D., Renzini A., Pope A., Alexander D. M., Bauer F. E., Giavalisco M., Huynh M., Kurk J., Mignoli M., 2007, ApJ, 670, 156

Draine B. T., Li A., 2007, ApJ, 657, 810

Elbaz D., Daddi E., Le Borgne D., Dickinson M., Alexander D. M., Chary R.-R., Starck J.-L., Brandt W. N., Kitzbichler M., MacDonald E., Nonino M., Popesso P., Stern D., Vanzella E., 2007, A&A, 468, 33

Ferland G. J., Porter R. L., van Hoof P. A. M., Williams R. J. R., Abel N. P., Lykins M. L., Shaw G., Henney W. J., Stancil P. C., 2013, Rev. Mexicana Astron. Astrofis., 49, 137

Foreman-Mackey D., Hogg D. W., Lang D., Goodman J., 2013, PASP, 125, 306

Foreman-Mackey D., Sick J., Johnson B., 2014, 10.5281/zenodo.12157

Girardi L., Bertelli G., Bressan A., Chiosi C., Groenewegen M. A. T., Marigo P., Salasnich B., Weiss A., 2002, A&A, 391, 195

González V., Labbé I., Bouwens R. J., Illingworth G., Franx

M., Kriek M., Brammer G. B., 2010, ApJ, 713, 115

Goodman J., Weare J., 2010, CAMCS, 5, 65

Hou F., Goodman J., Hogg D. W., Weare J., Schwab C., 2012, ApJ, 745, 198

Mackay D. J. C., 2003, Information Theory, Inference and Learning Algorithms. Cambridge University Press

Martin D. C., Wyder T. K., Schiminovich D., Barlow T. A., Forster K., Friedman P. G., Morrissey P., Neff S. G., Seibert M., Small T., Welsh B. Y., Bianchi L., Donas J., Heckman T. M., Lee Y.-W., Madore B. F., Milliard B., Rich R. M., Szalay A. S., Yi S. K., 2007, ApJS, 173, 342

Noeske K. G., et al. 2007, ApJ, 660, L43

Peng Y.-j., et al. 2010, ApJ, 721, 193

Planck Collaboration Ade P. A. R., Aghanim N., Arnaud M., Ashdown M., Aumont J., Baccigalupi C., Banday A. J., Barreiro R. B., Bartlett J. G., et al. 2016, A&A, 594, A13

Schawinski K., Urry C. M., Simmons B. D., Fortson L., Kaviraj S., Keel W. C., Lintott C. J., Masters K. L., Nichol R. C., Sarzi M., Skibba R., Treister E., Willett K. W., Wong O. I., Yi S. K., 2014, MNRAS, 440, 889

Smethurst R. J., Lintott C. J., Simmons B. D., Schawinski K., Marshall P. J., Bamford S., Fortson L., Kaviraj S., Masters K. L., Melvin T., Nichol R. C., Skibba R. A., Willett K. W., 2015, MNRAS, 450, 435

Vazdekis A., Koleva M., Ricciardelli E., Röck B., Falcón-Barroso J., 2016, MNRAS, 463, 3409

Weiner B. J., Willmer C. N. A., Faber S. M., Harker J., Kassin S. A., Phillips A. C., Melbourne J., Metevier A. J., Vogt N. P., Koo D. C., 2006, ApJ, 653, 1049

Westfall K., in prep., ApJ